Toronto Metropolitan University

AE/ME 8138 – Computational Dynamics
Winter 2024
Course Project Report

Dynamic Modelling and Analysis of a Parallel Linkage System for a Morphing Winglet Mechanism

Author: Aman Gilani
Student No.: 500879895

Table of Contents

List of Tables

List of Tables

1. Introduction

In recent years of aviation, winglets have been a key area of research for aerospace engineers to study their aerodynamic and performance-inducing capabilities. They play a critical role in mitigating induced drag which is caused by the wing's finite span and the presence of wingtip vortices. The winglet design effectively reduced such disturbances by decreasing the strength and size of these vortices. Recent fluid simulations and flight tests for these wingtip structures have exhibited their favorable contribution to reducing fuel consumption and enhancing aircraft range. The mechanism fundamental for the operation of a winglet primarily alters the direction of the airflow around the wing to reduce the wingtip vortices effects. That is why, the wing-winglet interaction becomes an area of focus since the mechanism controlling the winglet cant angle should be strong enough to withstand the aerodynamic and structural loads as well as cozily fit inside the wing structure.

This project aims to model and analyze the motion of a parallel mechanism system that controls the cant angle of the winglet, enabling wing-morphing capabilities. The parallel mechanism is shown in **Figure 1**, it utilizes two linkages with opposite motion attached to a common end effector (Winglet), with one linear actuator in the extension link and another in the retraction link to achieve the cant motion of the winglet.

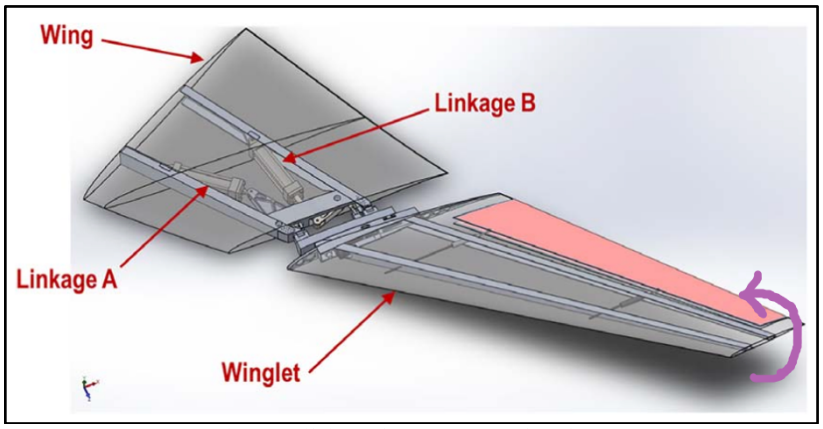

Figure 1: *Winglet Parallel Mechanism Housed in the Wing Structure.*

The parallel mechanism for a winglet cant actuation is designed to achieve greater payload capacity without sacrificing the mechanism's performance and efficiency. The design of a parallel mechanism for the purposes of controlling a winglet offers several advantages in terms of its stiffness, and payload capacity. Its characteristic stiffness, which results from the redundant constraints provided by the parallel links arrangement, ensures greater accuracy and strength in rotating the winglet. Additionally, its ability to handle heavy aerodynamics and structural loads while maintaining high rotation accuracy and speed is achieved by distributing the load among multiple actuators, Joints, and links.

The extension and retraction linkages are similar to each other in terms of their kinematic design, with 6 linkages and 7 joints each, making it a six-bar spatial linkage with a linear actuator. The mechanism translates the planar motion (X-Y Frame) of the linear actuator into a rotary motion (X-Z Frame) for the common end effector, in this case, the winglet. The joint types for each subsystem consist of three spherical joints, three revolute joints, and a prismatic joint that provides for the necessary actuation. The local Degree of Freedom (DOF) for the aforementioned joints are 3, 1, and 1 respectively. Thus, the complete DOF for each subsystem is calculated to be 13. Further, since the mechanism is a spatial system, the mobility of each subsystem is computed to be 1. Since the mobility of the subsystem is less than Lamda for a spatial system ($\lambda = 6$), the mechanism is defined as constrained with only one motor/actuator necessary for the motion of the mechanism. The mechanism is also defined as a closed-loop system since the end effector position does not change during the motion of the mechanism.

The objective for this project is to complete the dynamic modeling of the system using MATLAB resources and equations of motion developed in the class, to understand the machine's design, motion, and control. Firstly, the project will focus on computing the tool tip's (i.e. the winglet) position, orientation, and kinematics given a set of initial orientations, positions, velocities, and acceleration for each joint. This will be completed by utilizing the inverse kinematics methodology wherein the tip motion guides the analysis procedure to compute the base parameters mentioned above in the reverse order. Secondly, by using the calculated motion parameters mentioned above, the analysis will employ the Euler-Newton Recursive method to calculate the joint forces under each joint's self-weight and the given payload weight and tip force. Finally, the study will use these computed parameters to simulate the mechanism that incorporates the joint position, velocity, and acceleration.

2. Mobility Analysis

In this project, the mobility analysis of the chosen parallel mechanism is divided into halves for the sole purpose of similarity. Hence, a similar analysis for Linkage A will also apply to Linkage B due to symmetry in their operation. As seen in **Figure 2**, the kinematic architecture of the parallel mechanism incorporates spherical joints, revolute joints, and a prismatic joint connected by links to a common end effector that rotates about a common axis of rotation. This configuration makes the system a six-bar spatial linkage with a linear actuator. The input for the linear actuator is applied in a planar (X-Y) frame and the rotary output for the common end effector is in a planar (X-Z) frame.

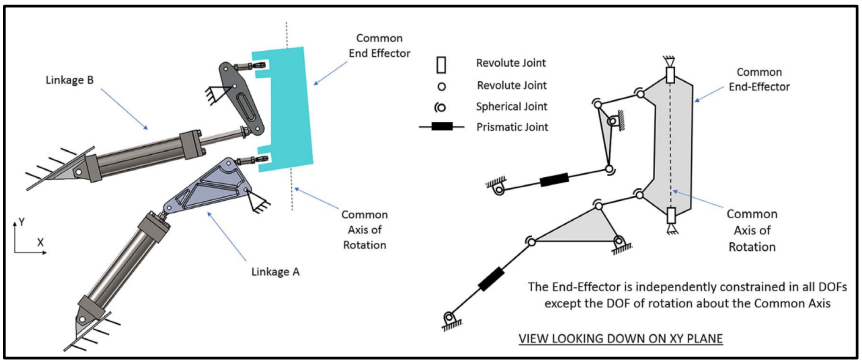

Figure 2: *Kinematic Architecture for the Two Branches of the Mechanism.*

For each linkage, there are 7 joints and 6 links. The three spherical joints have a local DOF of 3 each. The three revolute joints have a local DOF of 1 and finally, the prismatic joint has a local DOF of 1 as well. Using the kinematic pair information, the total degree of freedom for the system is calculated to be 13 and the mobility of the system is calculated to be 1 for this spatial mechanism. Linkages A and B have similar kinematic structures and therefore will have the same DOF and mobility. However, due to their spatial constrain and parallel similarity, they will have opposing motions. To illustrate this, if the linear actuator for Linkage A extends, the linear actuator of Linkage B will retract to provide for the rotation of the common end effector about a common axis of rotation. Therefore, the purpose of this parallel actuation is to provide for a desired rotation of the common end effector at a prearranged angular speed.

The kinematic modeling for a branch is completed using inverse kinematics, wherein, the end effector motion is predefined, and the joint kinematics is analyzed in reverse order to calculate the base parameters. The Linkage A branch model is illustrated in **Figure 3**. The system is further divided into two loops for the purpose of motion analysis only. The starting loop features the spatial rotational motion of the end effector in the X-Z frame. The spatial loop 1 is defined with points P6, P5, P4, and P3. The input angular motion of the end effector translates the motion of this loop into the translation motion of loop 2. The second loop is defined as a planar loop with motion in the X-Y frame. The planar motion then defines the motion of the linear actuator. Loop 2 is defined by points P1, P2, and P3. The rotation of point P6 rotates the links about point 3 which then drives the linear actuator. This process is also known as inverse kinematics which is used to calculate the position, velocity, and acceleration of each joint.

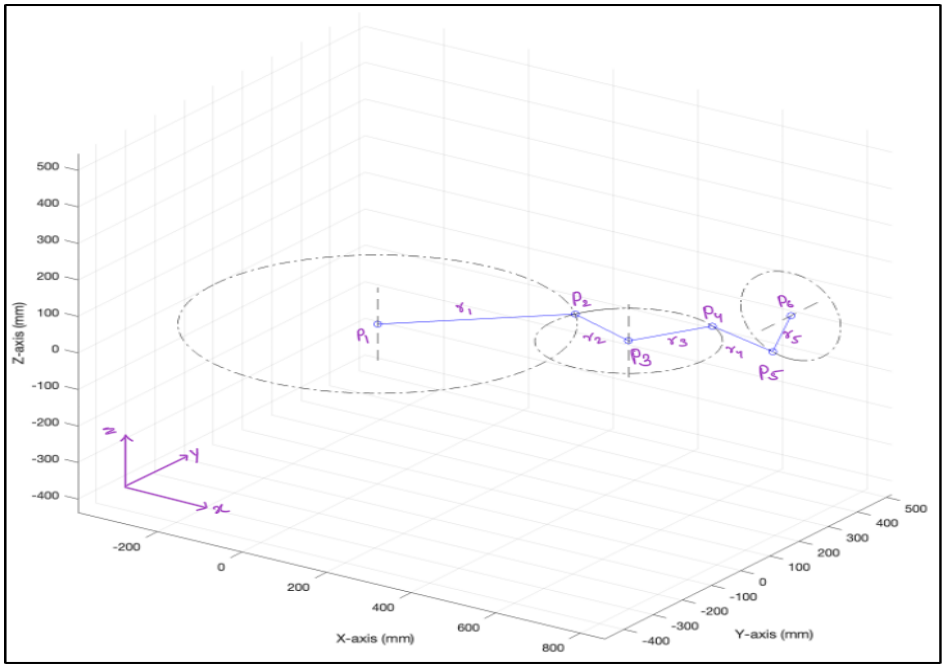

Figure 3: *Isometric View of Linkage A Branch with Joint-Link Pairs for Kinematic Modelling.*

The rotation of the end effector is about point P6. Therefore, the motion of point P5 is planar in the X-Z frame. On the other hand, the rotation of point P3 in planar loop 2 drives point P4 in the X-Y frame. Therefore, despite using spherical joints placed at points P2, P4, and P5 their motion is entirely planar. This is one of the limitations of analyzing the mechanism analytically. However, the planar motion for spherical joints simplifies the following kinematic analysis of the mechanism.

Figure 4 illustrates Linkage A in its top view (left) and side view (right). The top view depicts the planar loop 2 with a linear actuator placed between points P1 and P2. The figure also shows the circular trajectory of point P4 and the motion in the X-Y frame. The side view illustrates the spatial loop 1 with a rotating motion of the end effector in the X-Z frame. The figure also shows the circular trajectory of point P6 (end effector). Each loop consists of three links. The linear actuator is represented by r1. The triangular link is denoted by r2 and r3. The spatial link is denoted by r4, and the end effector link is represented by r5 with a rotation angle of θ_6.

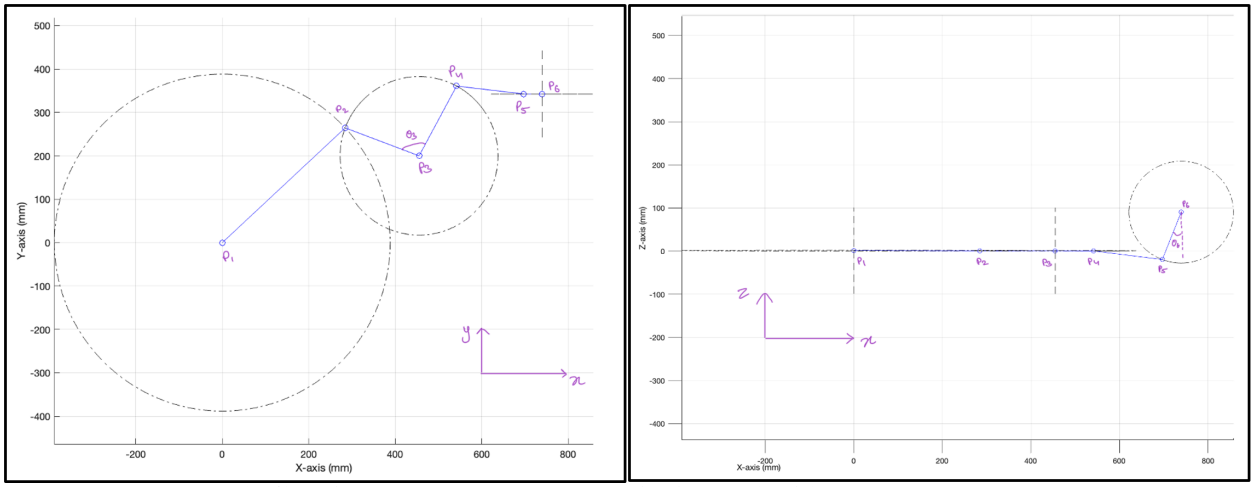

Figure 4: *Top View (Left) – Planar Motion in X-Y Frame, and Side View (Right) – Rotating Output Motion in X-Z Frame.*

3. Coordinate System

In analyzing a mechanism, the next important step is to define the coordinate frames for the number and type of joints. The coordinate frames are defined for each 'n+1' joint relative to the relative 'n' joint, and the base 'n_o' joint is defined relative to the global frame. **Figure 5** illustrates the stick figure of the mechanism with link and joint nomenclature. The total number of joints is 7 and the total number of links is 6 including the ground link. Joints J1, J4, and J7 depict revolute joints with one DOF each and rotation about their local z-axis. Joints J3, J5, and J6 depict spherical joints with three DOF each with a rotation about the X&Y axis for Joints J3 and J5 and a rotation about the X&Z axis for Joint J6. Finally, Joint J2 depicts the prismatic joint with one DOF which represents a linear actuator in the mechanism. The linear motion of the actuator is in its local Z axis. The coordinate frame for the position analysis is illustrated in **Figure 5**. The static and motion rotation for each joint is further determined to compute the base rotation angle for joint J1 in the inverse kinematics method.

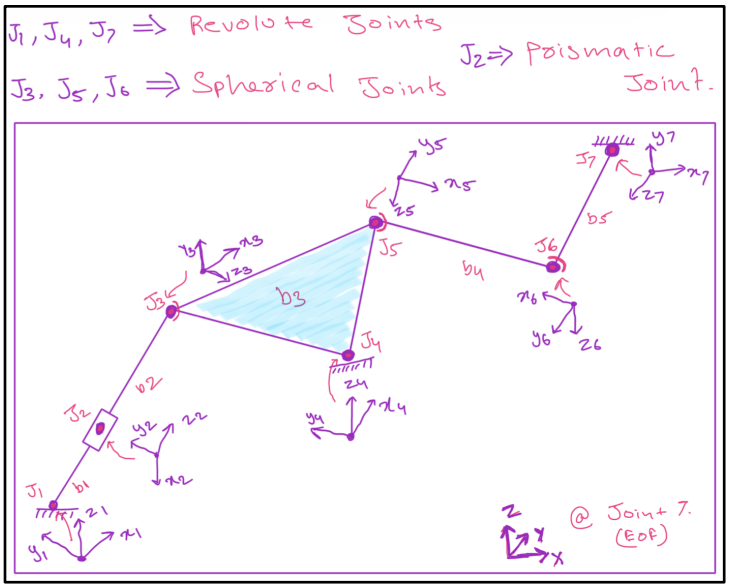

***Figure 5**: Stick Figure for the proposed Linkage A Branch with Link and Joint nomenclature.*

Further, the coordinate frames for the mechanism are divided into four branches presented in **Figure 6**. This is done due to the system being a closed chain loop. The joint velocity, acceleration, and forces are computed using this branched coordinate system. The branching follows the inverse analysis direction as well. Branch 1 consists of 2 links and 1 joint, which is the end effector revolute joint. The motion of the end effector is given in degrees with a rotation about the local Z axis along with its angular velocity, acceleration, and base forces. The dynamic motion of joint J6 is then computed using the given end effector inputs. Branch 2 consists of 3 links and 2 joints. Using the calculated dynamic motion of joint J6, the dynamic analysis of joints J4 and J5 is calculated. Branch 3 consists of 2 links and 1 joint. The base rotation and dynamic characteristics for joint J4 are similar in branches 2 and 3. Thus the dynamic motion of joint J3 is calculated using the joint J4 rotation, angular velocity, acceleration, and forces. The motion of joint J3 drives the linear actuator and rotates the revolute joint at position P1. The linear displacement, velocity, and acceleration of the linear actuator (prismatic joint) are calculated using the dynamic motion of joint J3.

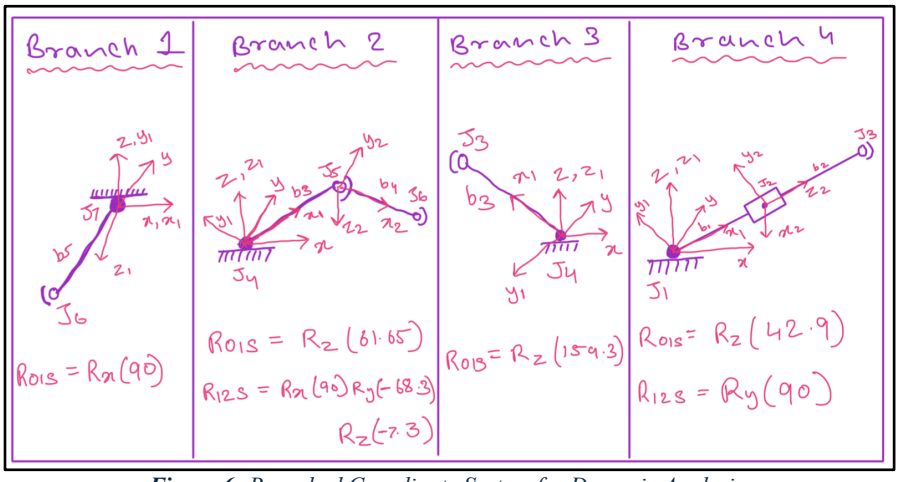

***Figure 6:** Branched Coordinate System for Dynamic Analysis.*

Figure 6 represents the 4 branches developed for the dynamic analysis. The branches consist of their respective coordinate frame system at each joint along with their static rotations matrices. **Table 1** tabulates the static rotation matrices for each joint and the local body vectors for each link in the branched coordinate frame system for the dynamic analysis. The body vectors are presented with respect to their local coordinate frame. The local body vectors can be multiplied by the respective static rotation matrix to calculate the body vector of the link in the global frame. The following equations are used to calculate the global body vector for each link and the position of each joint in the global frame. Note, that the end effector joint J7 and the base joint J1 are always fixed since the mechanism is a closed-loop system.

$$b_i = R_{0is} * b_i'$$

$$P_{n+1,static} = \sum_{i=0}^{n} b_i$$

Table 1: *Static Rotation Matrix and Local Static Body Vectors.*

	Branch 1	**Branch 2**	**Branch 3**	**Branch 4**
Static Rotation Matrix (R_s)	$R_{01s} = \begin{bmatrix} 1 & 0 & 0 \\ 0 & 0 & -1 \\ 0 & 1 & 0 \end{bmatrix}$	$R_{01s} = \begin{bmatrix} 0.4748 & -0.8801 & 0 \\ 0.801 & 0.4748 & 0 \\ 0 & 0 & 1 \end{bmatrix}$ $R_{12s} = \begin{bmatrix} 0.3660 & 0.0469 & -0.9294 \\ -0.9219 & -0.1181 & -0.3690 \\ -0.1270 & 0.9919 & 0 \end{bmatrix}$	$R_{01s} = \begin{bmatrix} -0.9358 & -0.3526 & 0 \\ 0.3526 & -0.9358 & 0 \\ 0 & 0 & 1 \end{bmatrix}$	$R_{01s} = \begin{bmatrix} 0.7324 & -0.6809 & 0 \\ 0.6809 & 0.7324 & 0 \\ 0 & 0 & 1 \end{bmatrix}$ $R_{12s} = \begin{bmatrix} 0 & 0 & 1 \\ 0 & 1 & 0 \\ -1 & 0 & 0 \end{bmatrix}$
Local Body Vector (b_n') (mm)	$b_{1s}' = [-42.7 \quad -110 \quad 0]'$	$b_{1s}' = [182.6 \quad 0 \quad 0]'$ $b_{2s}' = [157.4 \quad 0 \quad 0]'$	$b_{1s}' = [182.6 \quad 0 \quad 0]'$	$b_{1s}' = [58.97 \quad 0 \quad 0]'$ $b_{2s}' = [0 \quad 0 \quad 329.13]'$

4. Position Analysis

The position analysis is completed using the inverse kinematics of the mechanism. In this analysis, the rotation of the end effector (P6 or J7) in the X-Z frame is given by an angle θ_6. For analysis purposes, this angle is assumed as 30 degrees. The pre-defined θ_6 will give the orientation for the end effector which then drives the linear actuator at joint J2. The stroke length of the linear actuator is denoted by length r1 in **Figure 3**. As illustrated in **Figures 3&4**, the rotation of the end effector in the X-Z frame drives the linear actuator in the X-Y frame.

4.1 Position

Since the position of point P6 for the end effector is stationary, vector P6 is always known. With the change in angle θ_6, the location of point P5 is calculated by the following relationship:

$$\boldsymbol{P_5} = \boldsymbol{P_6} - \begin{bmatrix} r_6 * \sin(\theta_6) \\ 0 \\ r_6 * \cos(\theta_6) \end{bmatrix}$$

Point P3 is fixed, therefore vector P3 is always constant. Using the calculated position of point P5, the link magnitudes r3 and r4 are calculated using the following relationships. The z-

component of point P4 is always zero since it is a part of the planar loop 2. Therefore, the system of two unknows (X&Y component of P4) are solved simultaneously using two equations:

$$r_5 = |\boldsymbol{P_5} - \boldsymbol{P_4}|$$

$$r_4 = |\boldsymbol{P_3} - \boldsymbol{P_4}|$$

As seen in **Figure 3**, the points P4 and P2 are located on the same triangular link. They are separated by the following rotation matrix with a rotation of $R_z(\theta_3)$.

$$\boldsymbol{R}_2 = \begin{bmatrix} \cos(\theta_3) & -\sin(\theta_3) & 0 \\ \sin(\theta_3) & \cos(\theta_3) & 0 \\ 0 & 0 & 1 \end{bmatrix}$$

The unit vector for link r3 is then multiplied by the above rotation matrix and the length r2 to calculate the change in position of the triangular link with respect to the pre-defined rotation of end effector angle θ_6.

$$\boldsymbol{U}_{34} = \frac{\boldsymbol{P_3} - \boldsymbol{P_4}}{r_3}$$

$$\boldsymbol{P_2} = \boldsymbol{P_3} - r_2 \boldsymbol{R}_2 \boldsymbol{U}_{34}$$

Lastly, the linear actuator length r1 is then calculated by the following relation. This completes the position analysis using the inverse kinematics. As the end effector rotates with θ_6, the above equations are used to calculate the position for each point and the stroke length of the linear actuator.

$$r_1 = |\boldsymbol{P_2}|$$

The initial positions and final positions are for each joint are calculated and tabulated in **Table 2**. As seen, joints J1, J4, and J7 are fixed in space. The prismatic joint is located at joint J2, therefore, the link between joints J2 and J3 acts as a linear actuator.

Table 2: *Initial and Final Positions for Joints 1 to 7 using Inverse Kinematics.*

	Initial Positions (mm)	**Final Positions (mm)**
Joint 1	$[0 \quad 0 \quad 0]'$	$[0 \quad 0 \quad 0]'$
Joint 2	$[43.2 \quad 40.1 \quad 0]'$	$[104.4 \quad 148 \quad 0]'$
Joint 3	$[284.1 \quad 264.4 \quad 0]'$	$[336.6 \quad 339.1 \quad 0]'$
Joint 4	$[455 \quad 200 \quad 0]'$	$[455 \quad 200 \quad 0]'$
Joint 5	$[541.7 \quad 360.7 \quad 0]'$	$[608.6 \quad 298.7 \quad 0]'$
Joint 6	$[696.8 \quad 342.5 \quad 0]'$	$[757.5 \quad 342.5 \quad -26]'$
Joint 7	$[739.5 \quad 342.5 \quad 90]'$	$[739.5 \quad 342.5 \quad 90]'$

The results for the position analysis are illustrated by the mechanism diagram in **Figure 7**. The graph shows static and motion configurations for the mechanism as seen in the legend. The two configurations compare the change in position for joints J2, J3, J5, and J6. Joint J2 being the linear actuator, the extension of the actuator stroke is visible in the red. This linear motion of r1 is achievable due to the motion of end effector with an angle θ_6 in X-Z frame about the local Z-axis.

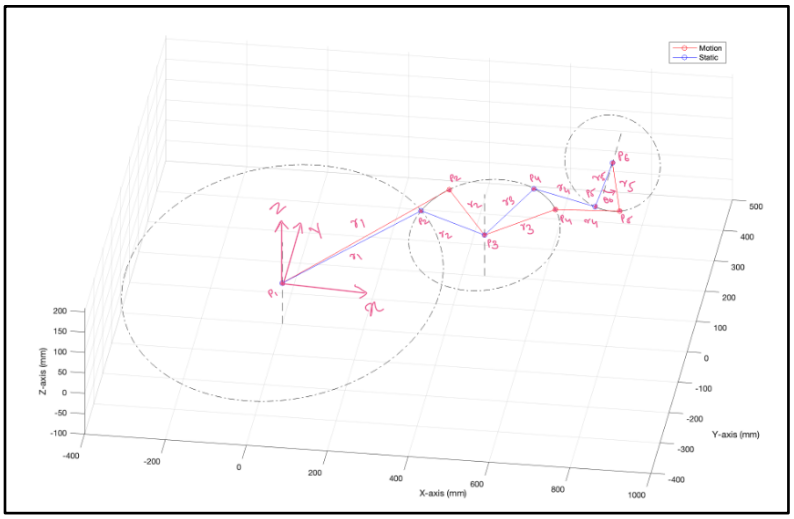

Figure 7: *Static and Motion Results for Position Analysis.*

4.2 Orientation

Subsequent to defining the static rotation matrices and local body vectors as tabulated in **Table 1**. The final orientation of the joints is calculated by defining motion rotation matrices and motion body vectors for each joint in each branch. Since the system is divided into four branches as described in **Figure 6**, the calculation follows the inverse kinematics scheme. Firstly, the rotation of the end effector in X-Z frame is defined with a motion of 30 degrees for θ_6 about its local Z-axis. The motion rotation matrices and motion body vectors are defined in **Table 3**.

Table 3: *Motion Rotation Matrix and Local Motion Body Vector.*

	Branch 1	**Branch 2**	**Branch 3**	**Branch 4**
Motion Rotation Matrix (R_m)	$R_{1m} = \begin{bmatrix} 0.866 & -0.5 & 0 \\ 0.5 & 0.866 & 0 \\ 0 & 0 & 1 \end{bmatrix}$	$R_{1m} = \begin{bmatrix} 0.8751 & 0.4840 & 0 \\ -0.4840 & 0.8751 & 0 \\ 0 & 0 & 1 \end{bmatrix}$ $R_{2m} = \begin{bmatrix} 0.623 & 0.144 & 0.770 \\ -0.091 & 0.990 & -0.11 \\ -0.777 & 0 & 0.629 \end{bmatrix}$	$R_{1m} = \begin{bmatrix} 0.8751 & 0.4840 & 0 \\ -0.4840 & 0.8751 & 0 \\ 0 & 0 & 1 \end{bmatrix}$	$R_{1m} = \begin{bmatrix} 0.9992 & -0.0401 & 0 \\ 0.0401 & 0.9992 & 0 \\ 0 & 0 & 1 \end{bmatrix}$ $R_{2m} = \begin{bmatrix} 1 & 0 & 0 \\ 0 & 1 & 0 \\ 0 & 0 & 1 \end{bmatrix}$
Motion Body Vector ($b_{m,n}$) (mm)	$b'_{1m} = [0 \quad 0 \quad 0]'$	$b'_{1m} = [0 \quad 0 \quad 0]'$ $b'_{2m} = [0 \quad 0 \quad 0]'$	$b'_{1m} = [0 \quad 0 \quad 0]'$	$b'_{1m} = [0 \quad 0 \quad 0]'$ $b'_{2m} = [0 \quad 0 \quad 89]'$

The motion rotation matrices and motion body vectors in **Table 3** are used to calculate the tip orientation and tip position for each branch. The following relationships are used for this calculation. Note that the calculated tip position vectors are different from the position vectors presented in the position analysis (**Section 5.1 – Table 2**). This is because the location of the global coordinate frame for each branch is different from the location of the coordinate frame used to complete the position analysis. Thus, the definition of the subsequent rotation matrices is also different. The tip rotation matrices and tip position vectors for the four branches are tabulated in **Table 4**. To check if the position vectors are correct, they can be transformed back to the global coordinate frame at joint J1 and cross checked with the position vectors tabulated in **Table 2**.

$$b_i = R_{0is} * R_{im} * b'_i$$

$$P_{n+1,motion} = \sum_{i=0}^{n} b_i$$

Table 4: *Tip Orientation and Tip Position.*

	Branch 1	Branch 2	Branch 3	Branch 4
Tip Orientation (R_{ot})	$\begin{bmatrix} 0.866 & -0.5 & 0 \\ 0 & 0 & -1 \\ 0.5 & 0.866 & 0 \end{bmatrix}$	$\begin{bmatrix} 0.945 & 0.218 & 0.242 \\ 0.278 & -0.156 & -0.947 \\ -0.169 & 0.963 & -0.209 \end{bmatrix}$	$\begin{bmatrix} -0.648 & -0.762 & 0 \\ 0.762 & -0.648 & 0 \\ 0 & 0 & 1 \end{bmatrix}$	$\begin{bmatrix} 0 & -0.7102 & 0.7040 \\ 0 & 0.7040 & 0.7102 \\ -1 & 0 & 0 \end{bmatrix}$
Tip Position (R_{n+1}) (mm)	$[18.02 \quad 0 \quad -116.6]'$	$[302.5 \quad 142.5 \quad -26.6]'$	$[-118.4 \quad 139.1 \quad 0]'$	$[335.9 \quad 338.8 \quad 0]'$

5. Motion Analysis

The motion analysis continues with computing the joint velocities and accelerations. The equation for angular and linear velocity and acceleration are derived similarly to the inverse kinematics methodology for position analysis in **Section 5.1**. For the motion analysis, the angular velocity and angular acceleration for the end effector and point P6 (joint J7) are pre-defined. For this analysis, the angular velocity (ω_6) is assumed to be 1 deg/s, and the angular acceleration (α_6) is assumed to be 1 deg/s^2. The linear velocity and acceleration for the linear actuator from loop 2 are calculated using the predefined joint J7 parameters (θ_6, ω_6, and α_6), and the inverse kinematics defined in the next section.

5.1 Velocity Analysis

Similar to the position analysis, the derivation of velocity equations for each joint starts with an end effector to the linear actuator at joint J2 and base rotation at joint J1. The velocity at position P5 is calculated by taking a time derivative of its position relationship. The velocity vector for point P5 is as follows:

$$\boldsymbol{V}_5 = -r_6 * \omega_6 * \begin{bmatrix} \cos(\theta_6) \\ 0 \\ -\sin(\theta_6) \end{bmatrix}$$

Furthermore, taking a time derivative of magnitude equations for r3 and r4 and then simultaneously solving them gives the velocity vector for point P4. Note that since the z-component for the position vector at point P4 is zero, its velocity component will also be zero. Thus, the relationship becomes two unknowns with two equations. Additionally, the velocity at point P3 is zero since it is fixed in space.

$$(P_{4x} - P_{5x}) * (V_{4x} - V_{5x}) + \left(P_{4y} - P_{5y}\right) * \left(V_{4y}\right) + (P_{5z}) * (V_{5z}) = 0$$

$$(P_{3x} - P_{4x}) * (-V_{4x}) + \left(P_{3y} - P_{4y}\right) * \left(-V_{4y}\right) = 0$$

The velocity of point P2 can be calculated by taking the time derivative of its position relationship. The velocity vector for point P2 is calculated as follows:

$$\boldsymbol{V}_2 = r_2 * \boldsymbol{R}_2 * \frac{\boldsymbol{V}_4}{r_3}$$

However, to calculate the stroke length, velocity, and acceleration of the linear actuator, the control rate equation is derived using Jacobian formulations. Using the computed velocity vector V_2 and a control sample period of 1 sec, the Jacobian formulation and the control rate are as follows:

$$P_{2,i} = P_{2,i-1} - \boldsymbol{V}_{2,i} * (\Delta t)$$

$$\Delta V_{actuator} = \frac{\left|P_{2,i} - P_{2,i-1}\right|}{\Delta t}$$

The control rate equation defines the change in velocity of the actuator stroke. ΔV represents the change in stroke position corresponding to the sample period Δt. This velocity is proportional to the actuator linear velocity which is required for the end effector rotation motion at the defined angular velocity (ω_6 = 1 deg/s) as defined in the problem statement.

Table 5: *Angular Velocity and Linear Velocity for Joints.*

	Angular Velocity (deg/s)	**Linear Velocity (mm/s)**
Joint 1	$[0 \quad 0 \quad 2.2574]'$	$[0 \quad 0 \quad 0]'$
Joint 2	$[0 \quad 0 \quad 2.2575]'$	$[-1.6489 \quad 1.6378 \quad 0]'$
Joint 3	$[0 \quad 0 \quad 2.2575]'$	$[-5.482 \quad -4.667 \quad 0]'$
Joint 4	$[0 \quad 0 \quad 2.259]'$	$[0 \quad 0 \quad 0]'$
Joint 5	$[0 \quad 0 \quad 2.2575]'$	$[-3.890 \quad 6.057 \quad 0]'$
Joint 6	$[0 \quad -1.0027 \quad 0]'$	$[2.035 \quad 0 \quad 0.3145]'$
Joint 7	$[0 \quad 0 \quad 1]'$	$[0 \quad 0 \quad 0]'$

The angular and linear velocities for each joint were computed and tabulated in **Table 5.** As expected, the linear velocity for joints J7, J4, and J1 are zero since they are fixed in space. The angular velocity of joint J7 describes the end effector rotation in the X-Z plane about its local z-axis. This drives the linear actuator with a linear velocity of [-1.65 1.64 0] mm/s and joint with an angular velocity of 2.257 deg/s in its local z-axis.

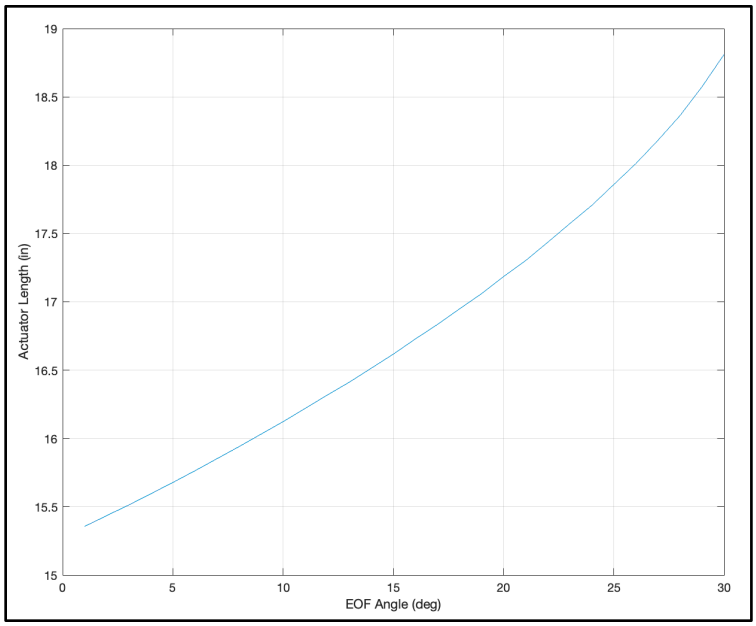

Figure 8: *Actuator Stroke Length Vs. End Effector Motion Angle.*

Figure 8 illustrates a significant graph that is used to compare the motion of the linear actuator with the end effector rotation. The figure plots the actuator stroke length (r1) versus the end effector rotation angle which is predefined at the beginning of the analysis. It was discovered that as the end effector angle increases from 0 to 30 with an increment of 1 deg/s, the linear actuator stroke increases proportionally. This trend was expected since linkage A is designed to extend throughout its motion limits.

5.2 Acceleration Analysis

The derivation of acceleration equations for each joint starts with the end effector to the linear actuator at joint J2 and base rotation at joint J1. The acceleration at position P5 is calculated by taking a time derivative of its velocity relationship. The acceleration vector for point P5 is as follows:

$$\boldsymbol{A}_5 = r_6 * \left[\omega_6^2 * \begin{bmatrix} \sin(\theta_6) \\ 0 \\ \cos(\theta_6) \end{bmatrix} - \dot{\omega}_6 * \begin{bmatrix} \cos(\theta_6) \\ 0 \\ -\sin(\theta_6) \end{bmatrix} \right]$$

Furthermore, taking a double time derivative of magnitude equations for r3 and r4 and then simultaneously solving them gives the acceleration vector for point P4. Note that since the z-component for the position vector at point P4 is zero, its acceleration component will also be zero. Thus, the relationship becomes two unknowns with two equations. Additionally, the acceleration at point P3 is zero since it is fixed in space. The acceleration for point P4 can be calculated by simultaneously solving the following equations.

$$V_{4y}^2 + \left(P_{4y} - P_{5y}\right) * A_{4y} + (A_{4x} - A_{5x}) * (P_{4x} - P_{5x}) + (V_{4x} - V_{5x})^2 + (P_{5z} * A_{5z}) + V_{5z}^2 = 0$$

$$V_{4x}^2 + V_{4y}^2 - (P_{3x} - P_{4x}) * A_{4x} - \left(P_{3y} - P_{4y}\right) * A_{4y} = 0$$

The acceleration of point P2 can be calculated by taking the double time derivative of its position relationship. The acceleration vector for point P2 is calculated as follows:

$$\boldsymbol{A}_2 = r_2 * \boldsymbol{R}_2 * \frac{\boldsymbol{A}_4}{r_3}$$

The stroke acceleration of the linear actuator is calculated by the control rate equation derived using Jacobian formulations. Using the computed acceleration vector A_2 and a control sample period of 1 sec, the Jacobian formulation and the control rate are as follows:

$$V_{2,i} = V_{2,i-1} - \boldsymbol{A}_{2,i} * (\Delta t)$$

$$\Delta A_{actuator} = \frac{\left|V_{2,i} - V_{2,i-1}\right|}{\Delta t}$$

The control rate equation defines the change in acceleration of the actuator stroke. ΔA represents the change in stroke velocity corresponding to the sample period Δt. This acceleration is proportional to the actuator linear acceleration which is required for the end effector rotation motion at the defined angular velocity (ω_6 = 1 deg/s) and angular acceleration ($\alpha_6 = 1\ \mathrm{deg/s^2}$) as defined in the problem statement.

Table 6: *Angular Acceleration and Linear Acceleration for Joints.*

	Angular Acceleration (deg/s²)	**Linear Acceleration (mm/s²)**
Joint 1	$[0 \quad 0 \quad 1.9309]'$	$[0 \quad 0 \quad 0]'$
Joint 2	$[0 \quad 0 \quad 1.9309]'$	$[-1.4749 \quad 1.3351 \quad 0]'$
Joint 3	$[0 \quad 0 \quad 1.9309]'$	$[-4.508 \quad -4.211 \quad 0]'$
Joint 4	$[0 \quad 0 \quad 1.933]'$	$[0 \quad 0 \quad 0]'$
Joint 5	$[0 \quad 0 \quad 1.9309]'$	$[-3.568 \quad 5.031 \quad 0]'$
Joint 6	$[0 \quad -1.0027 \quad 0]'$	$[2.029 \quad 0 \quad 0.35]'$
Joint 7	$[0 \quad 0 \quad 1]'$	$[0 \quad 0 \quad 0]'$

The angular and linear acceleration for each joint were computed and tabulated in **Table 6.** As expected, the linear acceleration for joint J7, J4, and J1 are zero since they are fixed in space. The angular acceleration of joint J7 describes the end effector rotation in X-Z plane about its local z-axis. This drives the linear actuator with a linear acceleration of [-1.47 1.33 0] mm/s² and joint with an angular acceleration of 1.93 deg/s² in its local z-axis.

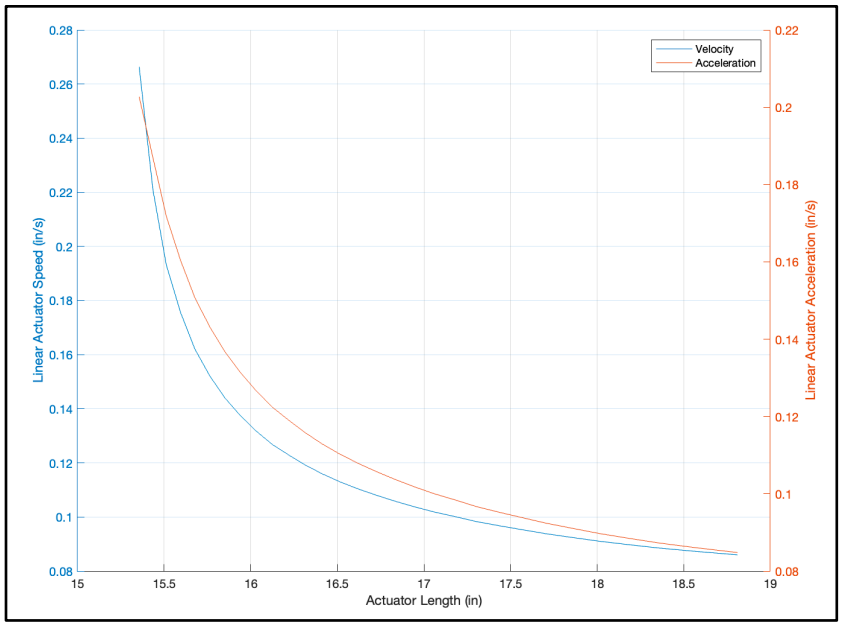

Figure 9: *Linear Actuator Speed and Acceleration Vs. Actuator Stroke Length.*

Figure 9 plots the linear stoke velocity and acceleration for the actuator versus the actuator stroke extension length. Following this, **Figure 10** plots the linear stoke velocity and acceleration for the actuator versus the end effector rotation angle. As the end effector angle increments from 0 to 30 degrees with an angular velocity of 1deg/s and an angular acceleration of 1deg/s^2, the linear actuator extends. As the actuator extends, the linear velocity and acceleration of the actuator follow a similar trend. These parameters start with a high enough velocity and acceleration to rotate the winglet and gradually slow down as the actuator end point (P2) reaches its final position. The significance of this velocity and acceleration control rate is used to understand the operation of linear actuators. A gradual decrease in the slope of the actuator's linear velocity and acceleration supports the structure from any impulse body forces thus making the morphing winglet motion seamless.

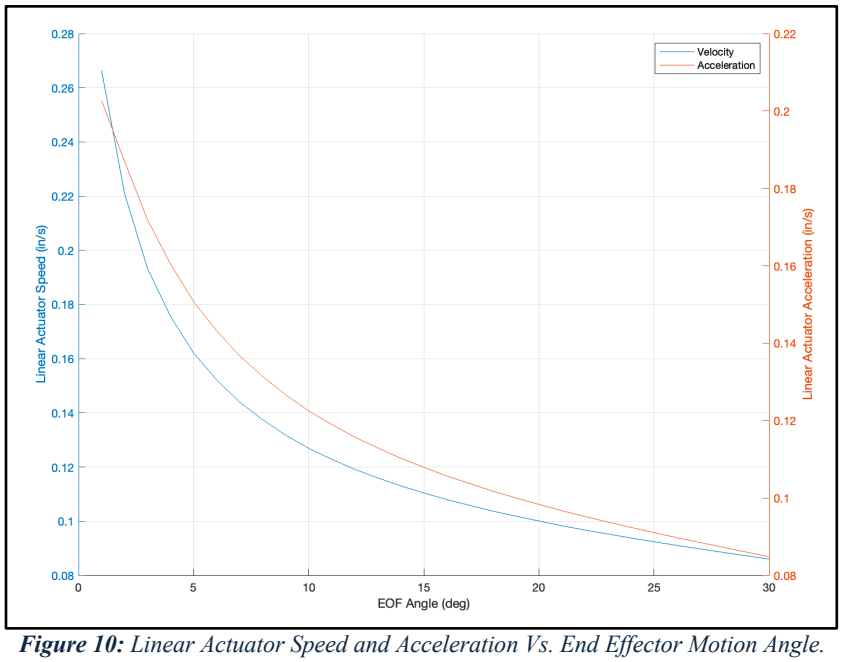

Figure 10: *Linear Actuator Speed and Acceleration Vs. End Effector Motion Angle.*

Table 7: *Position, Velocity, and Acceleration of the Linear Actuator at each Sample Period.*

Time (sec)	End Effector Rotation (deg)	Position (in)	Velocity (in/s)	Acceleration (in/s^2)
0	0	15.28	-	-
5	5	15.68	0.1621	0.1507
10	10	16.12	0.1269	0.1225
15	15	16.62	0.1104	0.1079
20	20	17.18	0.1001	0.0984
25	25	17.86	0.0920	0.0911
30	30	18.81	0.0860	0.0848

Table 7 tabulates the position, velocity, and acceleration of the linear actuator during the rotation of the end effector. The data presented is every 5 seconds, however, the parameters are computed every sample period of 1 sec. The data verifies **Figures 9&10.** As the linear actuator extends, from its static position of 15.28 inches to its final position of 18.81 inches, the end effector rotates 30 degrees. For the Linkage B mechanism, its actuator stroke length, velocity, and acceleration can be computed using a similar analysis discussed in the previous sections.

The position, velocity, and acceleration data computed here for the two branches is used to develop a basic CAD model for the entire parallel linkage mechanism. The parameters of this model are briefly described in **Section 7.**

6. Dynamic Analysis

The joint forces for the mechanism presented in **Figure 11** can be calculated following the completion of position analysis and motion analysis in the previous section. The forces, torques, and moments are calculated using the joint accelerations computed previously, the link's mass and moment of inertia, tip forces, and moments.

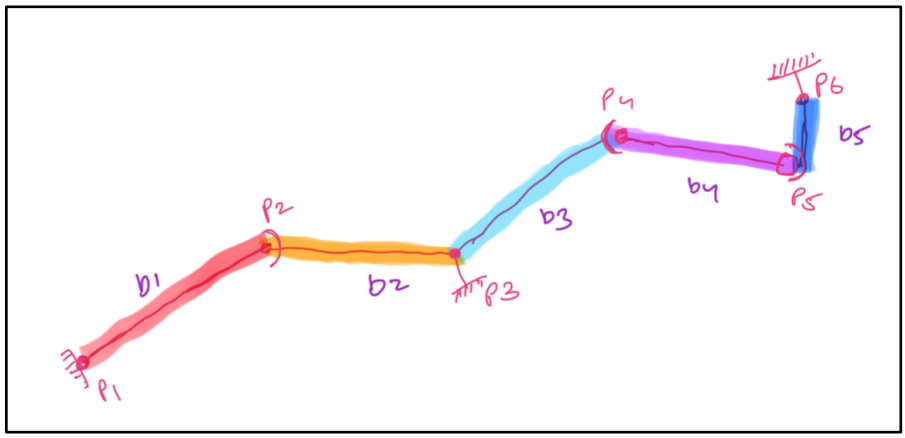

Figure 11: *Stick Figure of the Mechanism Indicating Body Vectors and Joint Nomenclature.*

The mass of each body is predefined, based on the material and volume of the link, and the moment of inertia is calculated using the body's mass, height, and radius. The body mass and moment of inertia are further tabulated in **Table 8**. The tabulated data follows the nomenclature defined in **Figure 11**.

Table 8: *Body Mass and Moment of Inertia.*

	Mass (kg)	Moment of Inertia (Kg.m^2)
Body 1	5	0.0633
Body 2	5	0.0144
Body 3	5	0.0144
Body 4	5	0.0108
Body 5	5	0.0063

Following defining the joint acceleration, mass, and moment of inertia for each body, the forces on each joint can be calculated for a static case and a dynamic case. The static case requires the payload and the mechanism to be in its initial configuration ($\theta_6 = 0^o$). Whereas the dynamic case requires the payload and the mechanism to be in its final configuration ($\theta_6 = 30^o$). After which, based on the payload case mentioned above, the lift forces, tip moment, and payload mass are defined.

6.1 Static Payload

The Static case requires the payload and the mechanism to be in its initial configuration ($\theta_6 = 0^o$) as seen below.

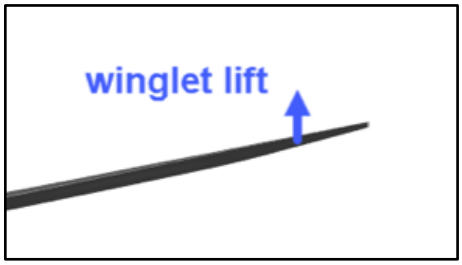

The lift forces, tip moment vector, payload mass, and gravitational acceleration vector are defined in **Table 9**. These parameters are used to calculate the joint forces for each branch using the recursive wrench computing method.

Table 9: *Tip Forces, Tip Moments, and Payload Mass.*

Lift	1000 N
Tip Force	$[0 \quad 0 \quad 1000]'$ N
Tip Moment	$[135 \quad 150 \quad 0]'$ N.m
Payload Mass	50 Kg
Gravitational Acceleration	$[0 \quad 0 \quad -10]'$ m/s^2

Table 10*: Joint Force and Moment Results for the Static Case.*

	Force (N) and Moment vector (N.m)
Branch 1	$\begin{matrix} & J5 & J6 \\ F_x & 0 & 0 \\ F_y & 0 & 0 \\ F_z = & -450 & -500 \\ M_x & -135 & -135 \\ M_y & 8.4 * 10^3 & -150 \\ M_z & 0 & 0 \end{matrix}$

	Force (N) and Moment vector (N.m)
Branch 2	$\begin{matrix} & J3 & J4 & J5 \\ F_x & 0 & 0 & 0 \\ F_y & 0 & 0 & 0 \\ F_z = & -400 & -450 & -500 \\ M_x & -62*10^3 & -20*10^3 & -135 \\ M_y & 135*10^3 & 70*10^3 & -150 \\ M_z & 0 & 0 & 0 \end{matrix}$
Branch 3	$\begin{matrix} & J3 & J2 \\ F_x & 0 & 0 \\ F_y & 0 & 0 \\ F_z = & -400 & -450 \\ M_x & -62*10^3 & -3*10^3 \\ M_y & 135*10^3 & 185*10^3 \\ M_z & 0 & 0 \end{matrix}$
Branch 4	$\begin{matrix} & J1 & J2 & J3 \\ F_x & 0 & 0 & 0 \\ F_y & 0 & 0 & 0 \\ F_z = & -350 & -400 & -450 \\ M_x & -44*10^3 & -129*10^3 & -3*10^3 \\ M_y & 326*10^3 & 310*10^3 & -185*10^3 \\ M_z & 0 & 0 & 0 \end{matrix}$

Table 10 tabulates the joint Force and Moment vectors in their global frames. As seen joint J1 experiences the lease force of -350 N in the global z-axis and the maximum moment of 326 kN.m about the global y-axis. Whereas the end effector joint J7 experiences a force of -500 N in its global z-axis and a moment of -135 kN.m about its global y-axis. The linear actuator joint J2 experiences a force of -400 N in the global z-axis and 310 kN.m moment about the global y-axis.

***Table 11**: Joint Local Forces and Torques.*

	Joint Forces (N)	Joint Torques (N.m)
Branch 1	$\begin{matrix} & J7 \\ F_x & -255 \\ F_y = & -389.7 \\ F_z & 0 \end{matrix}$	$\begin{matrix} & J7 \\ T_x & 116.9 \\ T_y = & 67.5 \\ T_z & 8.4*10^3 \end{matrix}$
Branch 2	$\begin{matrix} & J4 & J5 \\ F_x & 0 & 76 \\ F_y = & 0 & -433.5 \\ F_z & -400 & 93.9 \end{matrix}$	$\begin{matrix} & J4 & J5 \\ T_x & 20*10^3 & -169.4 \\ T_y = & 148*10^3 & -15*10^3 \\ T_z & 0 & -72*10^3 \end{matrix}$
Branch 4	$\begin{matrix} & J1 & J2 \\ F_x & 0 & 400 \\ F_y = & 0 & 0 \\ F_z & -350 & 0 \end{matrix}$	$\begin{matrix} & J1 & J2 \\ T_x & 129*10^3 & 0 \\ T_y = & 332*10^3 & 310*10^3 \\ T_z & 0 & 129*10^3 \end{matrix}$

Table 11 tabulates the local forces and torques acting on the joints. The local torque acting on the end effector joint J7 is [117 67 8400]' N.m. The local torque acting on the linear actuator joint J2 is [0 310 129]' kN.m.

Thus, the next step in this analysis is to complete a structural analysis of the parallel mechanism to check whether the links can sustain the applied forces. This is important to check because if the mechanism fails under the given loading, the entire wing can suffer catastrophic damage. In this project, only static analysis is considered since a dynamic analysis would require a calculation of the drag force's impact on the tip force and moment as well as the material's stiffness. The reasons for this are discussed further in **section 8**.

7. CAD Modelling

The results of position analysis are used to develop a CAD model on Solidworks. As seen in **Figure 12**, it shows a static configuration of the parallel mechanism where in $\theta_6 = 0^o$. The mechanism functions with the linear actuator driving the planar loop which rotates the winglet in an X-Z frame about the z-axis.

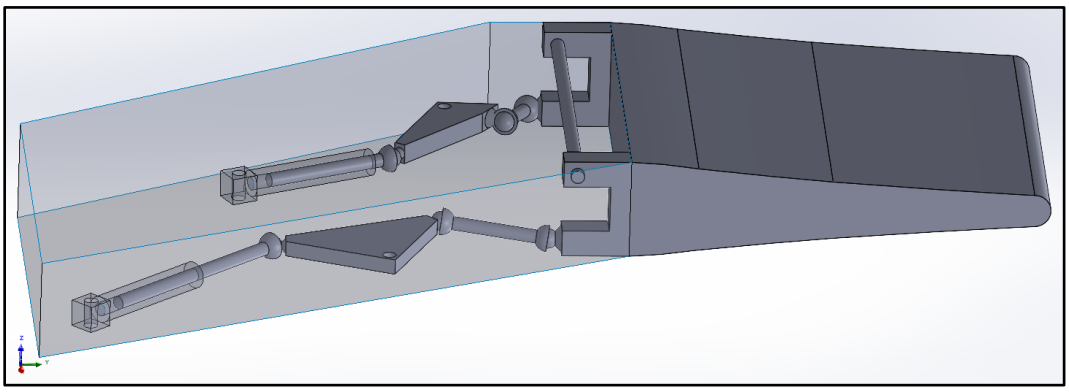

Figure 12: *CAD Model of the Parallel Mechanism at Static Configuration.*

Figure 13 illustrates the final configuration of the parallel linkage mechanism, wherein $\theta_6 = 30^o$.

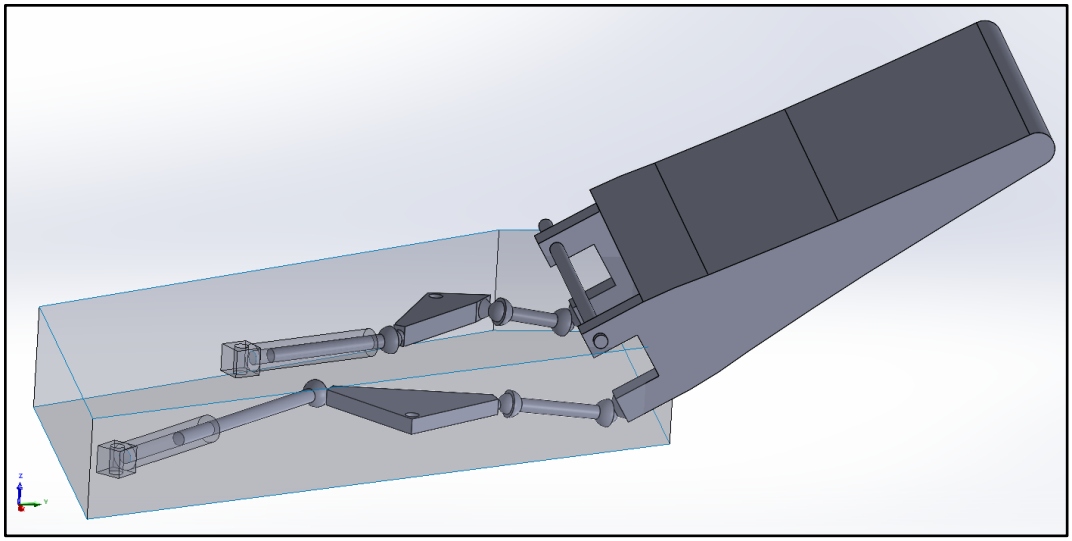

Figure 13: *CAD Model of the Parallel Mechanism at Final Configuration.*

8. Discussion

The main objective of this project is to complete a dynamic modeling and analysis of a parallel linkage system using basic computational dynamics knowledge and resources learned during the course. The operation of this mechanism was simplified well beyond how this system would actually function. The motion of the initial planar loop was considered to be in the X-Y frame only and the motion of the end effector rotation was to be in the X-Z frame. This simplified the motion of the spherical joints located at joints J3 and J5. This is why, their calculated positions are in X-Y plana and not spatial. However, in reality, the motion of this mechanism requires a spatial motion at joints J3 and J5. This is one of the limitations of studying the mechanism analytically.

The actuators for the parallel mechanism were not analyzed to be synchronous in motion for this analysis. This assumption simplified the problem to be solved separately without any actuator stroke length, velocity, and acceleration constraints. However, for the function of this mechanism, the linear actuator for linkage A and linkage B should be synchronized to achieve an optimal motion of the end effector without any overlapping constraints. Additionally, the actuator control rate was set up independent of the forces and torques acting upon it. This is because, to set up a force-dependent control rate for the actuator, a control law would have to be designed that uses the forces in negative feedback to output an applicable actuator velocity and acceleration.

The aerodynamic forces and the payload weight forces were divided into halves before applying to the tip. This was done while assuming an equal distribution of forces over the two linkages. However, the ratio for force distribution can vary between 0.1 to 1 depending on the force feedback of the linear actuators, the position of the winglet, and other aerodynamic and aeroelastic parameters.

Lastly, the analysis does not account for any drag forces or aeroelastic acting on the winglet. Therefore, the dynamic payload calculations weren’t done. As this would require the equations to reflect a contribution from drag forces, material stiffness, contact forces, and joint acceleration.

9. Conclusion

In conclusion, this project aimed to comprehensively model a dynamic system using MATLAB resources and equations of motion developed in class. The primary focus was on understanding the design, motion, and control of the system, with specific attention given to computing the tool tip's position, orientation, and kinematics.

To achieve this, the project employed an inverse kinematics methodology, wherein the motion of the tool tip (winglet) guided the analysis procedure to compute the base parameters, including orientations, positions, velocities, and accelerations for each joint. This reverse-order approach facilitated a detailed understanding of how the system's components interact to produce the desired motion. The position analysis is completed using the inverse kinematics of the mechanism. In this analysis, the rotation of the end effector (P6 or J7) in the X-Z frame is given by an angle θ_6. For analysis purposes, this angle is assumed as 30 degrees. The pre-defined θ_6 will give the orientation for the end effector which then drives the linear actuator at joint J2. As the end effector angle increments from 0 to 30 degrees with an angular velocity of 1deg/s and an angular acceleration of 1deg/s^2, the linear actuator extends. As the actuator extends, the linear velocity and acceleration of the actuator follow a similar trend. These parameters start with a high enough velocity and acceleration to rotate the winglet and gradually slow down as the actuator end point (P2) reaches its final position.

Furthermore, the analysis utilized the Euler-Newton Recursive method to calculate the joint forces under the influence of self-weight, payload weight, and tip force. This step was crucial in understanding the forces acting on each joint and how they contribute to the overall system dynamics. The local torque acting on the end effector joint J7 is [117 67 8400]’ N.m. The local torque acting on the linear actuator joint J2 is [0 310 129]’ kN.m. The end effector joint J7 experiences a force of -500 N in its global z-axis and a moment of -135 kN.m about its global y-axis. The linear actuator joint J2 experiences a force of -400 N in the global z-axis and 310 kN.m moment about the global y-axis.

Overall, this project has provided a comprehensive understanding of the system's dynamics, from kinematics to forces and motion simulation. It serves as a solid foundation for future studies and applications in the field of mechanical engineering and robotics.

10. References

[1]
F. (Jeff) Xi, A. Moosavian, G. H. Campos, U. (Sana) Choudhuri, C. Z. (John) Sun, and R. Buchkazanian, "Analysis and Control of an Actuation-Redundant Parallel Mechanism Requiring Synchronization," *Journal of Mechanisms and Robotics*, vol. 12, no. 044501, Feb. 2020, doi: 10.1115/1.4045653.

[2]
R. C. Miake-Lye, M. Martinez-Sanchez, R. C. Brown, and C. E. Kolb, 'Plume and wake dynamics, mixing, and chemistry behind a high speed civil transport aircraft', *Journal of Aircraft*, vol. 30, no. 4, pp. 467–479, Jul. 1993, doi: 10.2514/3.46368.

[3]
L. Xu, Q. Li, N. Zhang, and Q. Chen, 'Mobility, Kinematic Analysis, and Dimensional Optimization of New Three-Degrees-of-Freedom Parallel Manipulator With Actuation Redundancy', *Journal of Mechanisms and Robotics*, vol. 9, no. 4, p. 041008, Aug. 2017, doi: 10.1115/1.4036517.

[4]
A. A. Shabana, *Computational dynamics*, 3rd ed. Chichester, West Sussex ; Hoboken: John Wiley & Sons, 2010.

[5]
D. H. Myszka, *Machines and mechanisms: applied kinematic analysis*, 4th ed. Boston: Prentice Hall, 2012.